Geophysical Research Letters

RESEARCH LETTER
10.1029/2018GL079944

Key Points:
- We observe daily and subdaily perturbations of seismic velocity associated with tides and solar heating using ambient seismic noise
- This demonstrates that crustal strain changes of the order of 10^{-8} can be monitored with a time resolution of 1 hr by dense seismic arrays
- Passive observations of seismic velocity changes are complementary to surface measurements and theoretical modeling of crustal deformation

Supporting Information:
- Supporting Information S1

Correspondence to:
S. Mao,
maos@mit.edu

Citation:
Mao, S., Campillo, M., van der Hilst, R. D., Brenguier, F., Stehly, L., & Hillers, G. (2019). High temporal resolution monitoring of small variations in crustal strain by dense seismic arrays. *Geophysical Research Letters, 46*, 128–137. https://doi.org/10.1029/2018GL079944

Received 6 AUG 2018
Accepted 20 NOV 2018
Accepted article online 28 NOV 2018
Published online 6 JAN 2019

©2018. American Geophysical Union. All Rights Reserved.

High Temporal Resolution Monitoring of Small Variations in Crustal Strain by Dense Seismic Arrays

Shujuan Mao[1], Michel Campillo[1,2], Robert D. van der Hilst[1], Florent Brenguier[2], Laurent Stehly[2], and Gregor Hillers[2,3]

[1]Department of Earth, Atmospheric and Planetary Sciences, Massachusetts Institute of Technology, Cambridge, MA, USA, [2]Institut des Sciences de la Terre (ISTerre), Université Grenoble Alpes, CNRS, IRD, Gières, France, [3]Now at Institute of Seismology, University of Helsinki, Helsinki, Finland

Abstract We demonstrate the feasibility of detecting very weak deformation in the shallow crust with high temporal resolution by monitoring the relative changes in seismic wave velocity (*dv/v*) using dense arrays of seismometers. We show that the *dv/v* variations are consistent between independent measurements from two seismic arrays. Dominant peaks in the observed *dv/v* spectrum suggest that tides and temperature changes are the major causes of daily and subdaily velocity changes, in accordance with theoretical strain modeling. Our analysis illustrates that *dv/v* perturbations of the order of 10^{-4}, corresponding to crustal strain changes of the order of 10^{-8}, can be measured from ambient seismic noise with a temporal resolution of 1 hr. This represents a low-cost technique for high precision and high time-resolution monitoring of crustal deformation that is complementary to existing geodetic measurements and is instrumental in both the detection and understanding of low-amplitude precursory processes of natural catastrophic events.

Plain Language Summary Theoretical and laboratory studies have shown that the onset of earthquakes, landslides, and volcanic eruptions is often preceded by a so-called *initiation phase*. Detecting such a precursory phenomenon will help in the prediction, early warning, or assessment of catastrophic geological events. The time scale and amplitude of these precursory evolutions are not well known, however, and their detection and characterization require monitoring techniques with both high precision and high temporal resolution. We present here an approach to monitor the elastic properties of crustal rocks using continuous recordings of ambient seismic noise by networks of dense autonomous sensors. We show that this technique allows the monitoring at a temporal resolution of 1 hr for crustal strain variations of the order of 10^{-8}, namely, the deformation associated with tides. This technique can be used in concert with existing geodetic techniques for understanding and detecting transient crustal deformation.

1. Introduction

Theoretical models and observational evidence suggest that the onset of instabilities responsible for earthquakes, landslides, and volcanic eruptions is often preceded by slowly evolving, low-amplitude initiation phases (Bouchon et al., 2011; Brenguier, Campillo, et al., 2008; Johnson & Jia, 2005; Scuderi et al., 2016; Tape et al., 2018). Both high temporal resolution and high precision measurement of crustal deformation are therefore crucial for hazard prediction and early warning.

Strain in the shallow subsurface can be inferred from geodetic data (e.g., Global Positioning System [GPS] and interferometric synthetic aperture radar [InSAR]) and other surface measurements (such as strainmeters or tiltmeters), or, alternatively, from relative variations in seismic wave velocity (*dv/v*) if data from dense seismograph arrays are available. Seismic velocity is sensitive to, for instance, strain associated with the closure or opening of cracks (Walsh, 1965). Traditional approaches to quantifying *dv/v* at subdaily time scales are limited by the need of repeating sources (Reasenberg & Aki, 1974; Yamamura et al., 2003; Wang, Zhu, et al., 2008). Here we demonstrate that temporal changes of *dv/v* can be detected and monitored with hourly resolution using continuous records of ambient seismic noise.

One can infer *dv/v* from time delays in the coda of the approximate Green's functions that are estimated from noise correlation at different times. This approach, which has been applied to various problems in geosciences (Brenguier et al., 2014; Brenguier, Campillo, et al., 2008; Brenguier, Shapiro, et al., 2008; Donaldson et al., 2017; Froment et al., 2013; Hillers, Retailleau, et al., 2015; Mordret et al., 2016; Olivier et al., 2015; Richter et al., 2014; Rivet et al., 2011; Sens-Schönfelder & Wegler, 2006; Wang et al., 2017), has

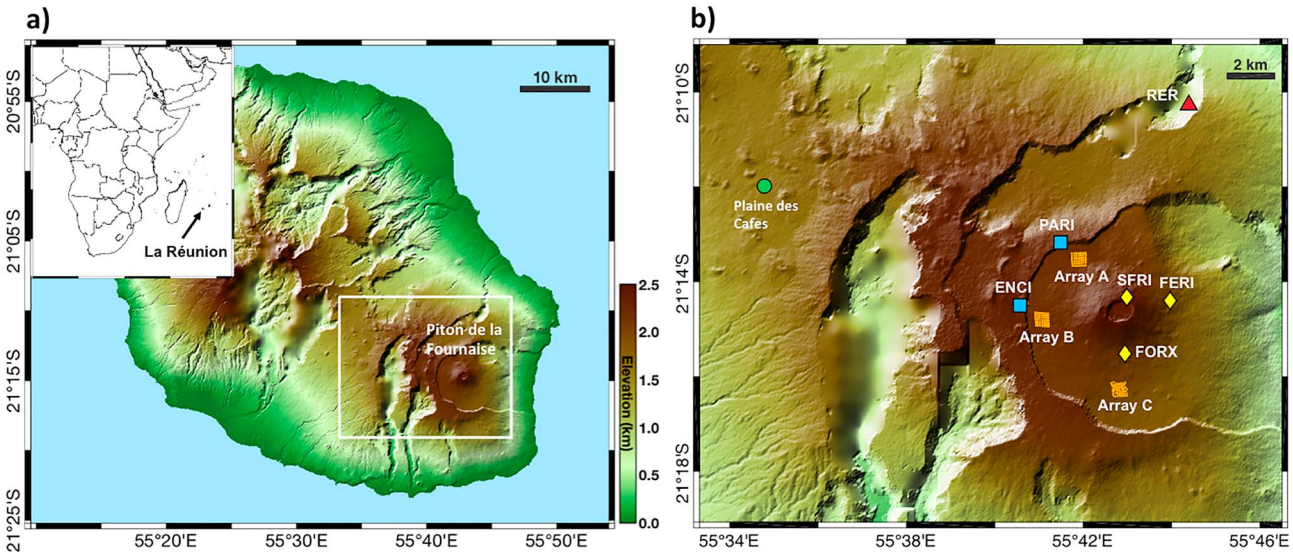


Figure 1. (a) Locations of La Réunion Island (inset) and Piton de la Fournaise volcano on La Réunion. (b) Locations of the receivers of the VolcArray seismic arrays (orange dots), the very broadband seismometer (red triangle), borehole tiltmeters (blue squares), the precipitation stations (yellow diamonds), and the meteorological station (green circle).

several advantages. First, the scattered seismic (coda) waves convey information about the average elastic properties of the subsurface volumes that they sample and are less affected by local heterogeneities compared with point measurements at Earth's surface. Second, it can be done continuously and at low costs, which is essential for long-term observation and monitoring of solid Earth. Furthermore, multiply scattered coda waves have a high sensitivity to changes in elastic properties in the shallow crust, providing a precision that is comparable to measurements from expensive active-source experiments.

Notwithstanding these advantages and the wide applicability, the noise-based monitoring of crustal strain still faces substantial challenges. The first is technical. Previous attempts with natural seismic noise involved stacking over long time windows in order to obtain a sufficient signal-to-noise ratio (Hillers, Ben-Zion, et al., 2015; Richter et al., 2014; Takano et al., 2014). The best temporal resolution achieved previously was ~1 day (Hadziioannou et al., 2011; Stehly et al., 2015) for monitoring of natural events. In many potential applications, such as prediction, early warning, or assessment of natural hazards, it is important to be able to detect changes on shorter time scales (e.g., a few hours or less). We achieve this by taking advantage of the newly available dense arrays of autonomous seismometers.

The second challenge concerns quantification and interpretation. Real-time change in seismic velocity is a relatively new type of observation, yet its relationship to strain has not been well established. Its multiple origins include tectonic deformation, water content perturbation, and temperature change, and isolating the effects of each mechanism is not easy. We meet this challenge by measuring the in situ responses of dv/v to reasonably well understood external forcings. By measuring the seismic velocity responses to predictable periodic strain (such as tides and solar heating) one can provide real-time information about the state of crustal rocks.

With seismic data from dense arrays at Piton de la Fournaise (PdF) volcano, La Réunion (Figure 1), we demonstrate that we can probe shallow crustal strain of the order of 10^{-8} at approximately hourly resolution and that at this site the inferred daily and subdaily variations in dv/v are due to tidal and thermal effects. Fine precision, high temporal resolution, and low costs together provide new possibilities for monitoring of geological processes in the shallow subsurface.

2. Data and Methods

2.1. The VolcArray Experiment

We use the seismic data from the VolcArray Experiment (Brenguier et al., 2016; Nakata et al., 2016) at PdF, La Réunion (Figure 1), which is one of the most active and best-instrumented volcanoes in the world. VolcArray

comprised three arrays that were placed a few kilometers from the Dolomieu crater and recorded ground motion continuously through July 2014, a quiet period of PdF. Each array had vertical component geophones (10-Hz corner frequency, 250-Hz sampling rate) on a 7 by 7 grid, with an average grid spacing of about 80 m and an aperture of about 0.5 km. The data from Arrays A and B are of high quality. However, the data quality for Array C is not sufficient for the purpose of this study, possibly because the sensors were not placed vertically due to the tough terrain and the bad weather condition on the day of deployment (as manifested by the irregular geometry of Array C), or because the sensors were not well coupled with the edifice due to the voids underneath Array C from lava flows south of the crater. In this paper we use data from Arrays A and B.

2.2. Noise-Based Monitoring of Seismic Velocity

Noise-based monitoring takes advantage of the possibility to estimate the Green's function, the seismic response to impulse source of the medium, by calculating cross correlations of ambient seismic noise recorded at two receivers (Campillo & Paul, 2003; Sabra et al., 2005; Shapiro & Campillo, 2004). The coda of these Green's functions is highly sensitive to small changes in the elastic properties of the medium (Poupinet et al., 1984; Snieder et al., 2002), and continuous Green's function reconstruction can be used to measure relative changes in arrival time (dt/t) of wave components, which yields dv/v.

We calculate the hourly noise cross correlations using preprocessing similar to Brenguier, Campillo, et al. (2008); that is, we down-sample the continuous noise data to 50 Hz and apply spectral whitening in the Fourier domain. Green's functions are then reconstructed by computing cross correlations for all of the station pairs within each array using the hourly noise data. We apply a two-dimensional Wiener filter to enhance the signal-to-noise ratio, with a filter order of 3 for both vertical (hour) and horizontal (time lag) dimensions (Wang, Tilmann, et al., 2008; Moreau et al., 2017) (see the supporting information). For each receiver pair, a reference cross-correlation function is obtained by stacking cross correlations for that pair over the entire study period. To calculate traveltime changes, we applied the Moving-Window Cross-Spectral Analysis (MWCSA; Clarke et al., 2011; Poupinet et al., 1984) to the coda in a 4- to 25-s window with high frequency 1–5 Hz of the reconstructed Green's functions. The relative wave velocity change is the opposite of the traveltime perturbation ($dv/v = -dt/t$). Errors in dv/v measurements are estimated following Weaver et al. (2011).

2.3. Simulations of Tide-Induced Strain

We simulated the tide-induced volumetric strain at PdF using the SPOTL program (Agnew, 2012). The simulations incorporate both the solid Earth tide and the ocean tidal loading. To compute the ocean tide, we use the global model osu.tpxo72atlas.2011 (Egbert & Erofeeva, 2002), with cell size of 0.125°, which is a hydrodynamic model assimilated with altimetry data. The east-west and north-south horizontal strain components are independently computed. Assuming a traction-free half space, the vertical strain component at the surface is then determined by the two horizontal components by $\varepsilon_{zz} = \zeta(\varepsilon_{xx} + \varepsilon_{yy})$, where $\zeta = -\nu/(1-\nu) = -1/3$ with Poisson's ratio $\nu = 1/4$. The total tide-induced volumetric strain is the sum of the vertical strain and horizontal strain.

3. Results

3.1. Temporal Variations of dv/v

The time series of dv/v averaged over the 1,225 station pairs are shown in Figure 2a. The measurements reveal relatively large variations (~0.05%) on time scales of days or weeks and smaller variations (~0.01%) on time scales of a day or less. The long-term changes could be associated with aseismic volcanic activity or precipitation (Figure 2b; Rivet et al., 2015). The daily and subdaily changes in dv/v are the major focus of this study.

A comparison of the yellow and blue lines in Figure 2a shows that the independent measurements from Arrays A and B match each other well for both long-term and short-term dv/v variations. We note that no major volcanic activity was recorded for PdF during this period, and we find no obvious dv/v correspondence to the three seismic events with magnitudes >2 that occurred in this time window (two M 2–3, one M 3.4).

3.2. Spectral Content of Daily and Subdaily Changes in dv/v

The spectral content of dv/v changes with time, but the spectrogram (Figure 2c) of dv/v in array B reveals distinct high-energy peaks at or near diurnal (1 cycle per day), semidiurnal (2 cycles per day), and terdiurnal

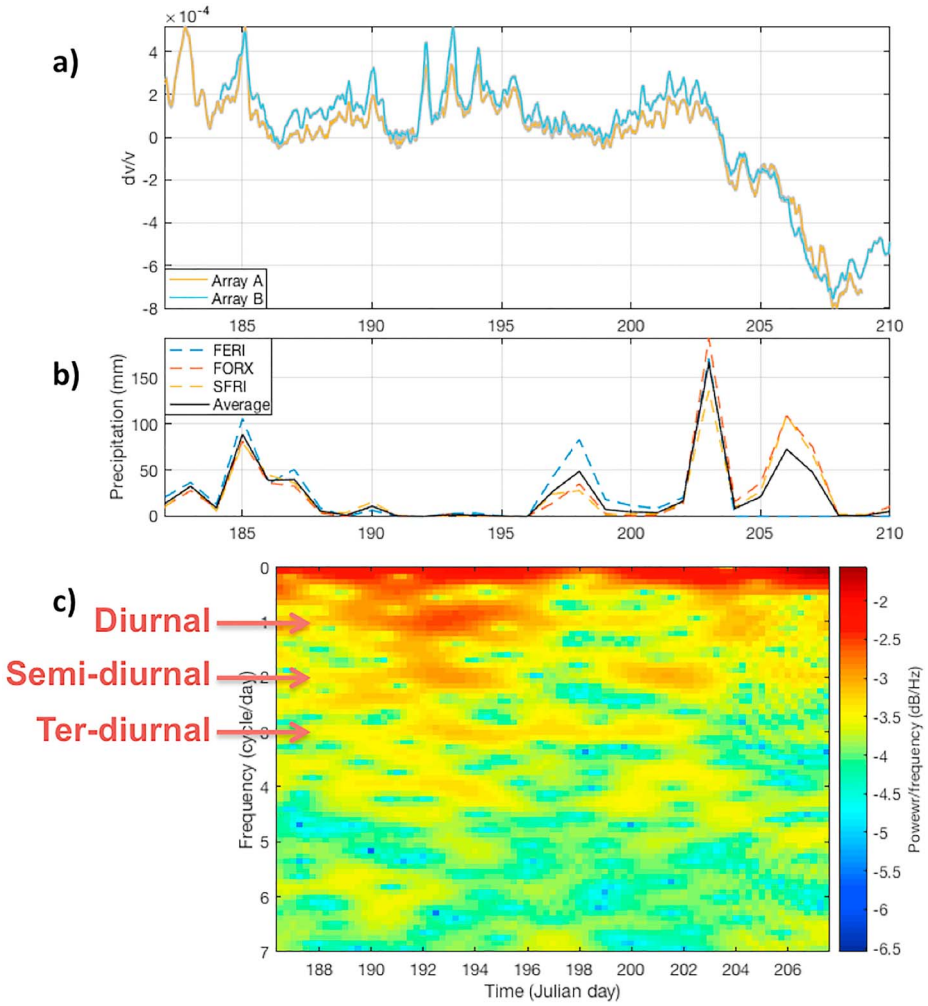


Figure 2. (a) The time series of relative seismic velocity changes (*dv/v*). The yellow line shows the average over 1225 station pairs of Array A from 1st to 27th July 2014, and the blue line shows the average of Array B from 3rd to 28th July 2014. The error of *dv/v* is indicated by grey shadow, which is about 1 order of magnitude smaller than *dv/v* itself. Within error the *dv/v* measurements from the two arrays are similar. (b) The precipitation at three stations FERI, FORX, and SFRI (Figure 1b) around the Dolomieu crater and their average. (c) The spectrogram of *dv/v* from Array B (corresponding to the time series in blue line in Figure 2a). Note the high-energy peaks at or near diurnal (1 cycle/day), semidiurnal (2 cycle/day), and terdiurnal (3 cycle/day) frequencies.

(3 cycles per day) frequencies. Calculation of the spectrum for the study period (analogous to stacking the spectrogram along the time axis in Figure 2c) enhances the peaks that correspond to the diurnal, semidiurnal, and terdiurnal frequencies (Figure 3a). To ensure that these spectral characteristics are robust and not related to spatiotemporal changes in the noise, we verify that the spectrum of the noise intensity (in 1- to 5-Hz frequency range as used in the MWCSA) does not show similar peaks (Figure S2).

Our measurements are stable for several reasons. First, the seismic coda recovered by cross correlation consists of multiply scattered waves and is much less sensitive than direct waves to directional changes in noise source distribution (Colombi et al., 2014; Hadziioannou et al., 2009). Second, averaging over station pairs at various azimuths helps reduce the potential bias in arrival times from reconstructed Green's functions due to uneven noise distribution. Indeed, we select groups of station pairs according to their azimuths and confirm that the *dv/v* measured over the study period is independent of the azimuth (Figure S3). Finally, the method that we use to infer arrival time changes (i.e., MWCSA) is based on phase measurements and is therefore not susceptible to changes in the noise amplitude spectrum (Zhan et al., 2013).

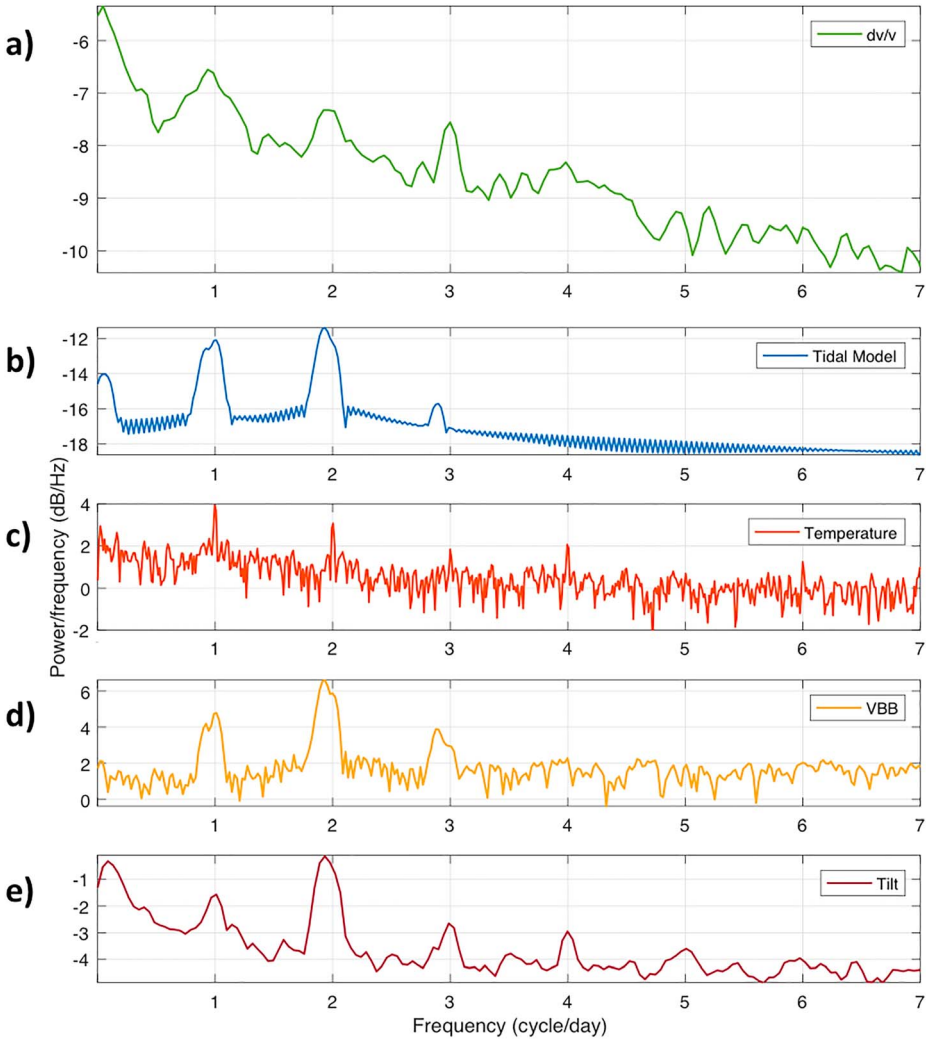


Figure 3. The spectra of five different types of data. From the top to the bottom are the spectra of (a) *dv/v*, (b) tidal volumetric strain modeled by SPOTL, (c) temperature records, (d) vertical acceleration records from the very broadband seismometer RER (Figure 1b), and (e) tilts from station PARI and ENCI (Figure 1b).

These observations suggest that the short-term changes and spectral characteristics (Figure 3a) of the obtained *dv/v* are not caused by spatiotemporal changes in the noise wavefield but by actual deformation of the shallow crust underneath the seismic arrays.

3.3. Possible Causes of Daily and Subdaily Variations in *dv/v*

At these frequencies (i.e., several cycles per day) prominent deformation in the shallow crust is caused by external forcings due to tides and solar radiation. First, the differential gravitational fields of the Moon, the Sun, and other celestial bodies result in the tidal deformation, comprising solid earth tides and ocean tide loading. Second, solar radiation causes daily temperature changes, inducing thermoelastic strain in the crust as well as variations in atmospheric pressure. On the one hand, the spatiotemporally varying temperature fields cause thermoelastic strain, which is larger in areas with extreme local topography and lateral material heterogeneity (Ben-Zion & Leary, 1986). Although the temperature changes themselves only penetrate tens to hundreds of centimeters into the crust, the thermoelastic strain can extend deeper (Berger, 1975; Ben-Zion & Leary, 1986; Tsai, 2011). On the other hand, the temperature-induced perturbations of atmospheric loading also lead to strain in the Earth.

To evaluate the imprints of tidal and thermal deformation on *dv/v*, in Figure 3 we compare *dv/v* (Figure 3a) with independent observations and modeling results. First, Figure 3b depicts simulations of tide-induced volumetric strains at PdF using the SPOTL program (Agnew, 2012). The main spectral peaks in Figure 3b are smooth and relatively broad because of the rich frequency constituents of tides (Melchior, 1974) and because the spectrum is computed over a finite time window. The modeled tidal spectrum reveals the well-known strong diurnal and semidiurnal peaks, with the latter larger than the former, and a weak terdiurnal peak.

Second, in Figure 3c we illustrate thermal effects by means of hourly temperature records from the nearby meteorological station at Plaine des Cafres (Figure 1b). The periodicity of solar heating is close to 1 day. As the shape of temperature change is not perfectly sinusoidal, its Fourier transform shows spikes at 1 cycle per day as well as higher order harmonics at 2, 3, 4, … cycles per day. In contrast to the tidal spectrum, in the temperature spectrum the diurnal thermal peak is larger than the semidiurnal thermal peak and the terdiurnal thermal peak is comparable to the first two peaks.

Finally, for comparison with our array estimates of *dv/v*, we display two other measures of ground deformation. In Figure 3d we display the spectrum of vertical acceleration from a very broadband STS-1 seismometer at GEOSCOPE station RER (Figure 1b). We note that at long periods the seismometer records both translational and rotational motions (Pillet & Virieux, 2007). In Figure 3e we use data from two borehole tiltmeters (PARI and ENCI) that are close to Arrays A and B (Figure 1b) and show the average spectra from horizontal pendulums at these stations.

All of the spectra in Figure 3 have prominent diurnal, semidiurnal, and terdiurnal peaks. Comparing the tidal and thermal spectra (Figures 3b and 3c) we notice that the diurnal and semidiurnal peaks, respectively, overlap, whereas the terdiurnal peaks occur at different frequencies. The other spectra—*dv/v* (Figure 3a), very broadband seismometer (Figure 3d), and tilt (Figure 3e)—seem to be affected by a combination of tidal and thermal effects, but the relative amplitudes depend on the frequency band. In the following we assess the contributions of tidal and thermal effects on *dv/v* and crustal strain.

3.4. Tidal and Thermal Effects on *dv/v*

3.4.1. Terdiurnal

The tide model shows a peak at a frequency (2.87 cycles per day, tidal constituent M_3) that differs substantially from the thermal signal (3 cycles per day) and which is much weaker than the peaks at 1 cycle per day and 2 cycles per day (Figure 3b). Well-defined terdiurnal peaks in the *dv/v* (Figure 3a) and tilt spectra (Figure 3e) coincide with the thermal peak at 3 cycles per day. These observations combine to suggest that the terdiurnal variations in *dv/v* are primarily due to thermal effects.

3.4.2. Semidiurnal

The semidiurnal *dv/v* and tilt peaks occur closer to the main tidal peak (just below 2 cycles per day) than the thermal peak (2 cycles per day). Furthermore, the time series (Figure 4a) shows that *dv/v* and tidal model (filtered in the semidiurnal band) are nearly in phase, which is only likely to happen if the *dv/v* is dominated by semidiurnal tide and if the relaxation time of *dv/v* in response to strain change is considerably shorter than semidiurnal period (see the supporting information). The phase relationship between *dv/v* and temperature-induced strain remains unknown, because neither the phase difference between temperature at the meteorological station and at the seismic array, nor the phase delay between temperature and thermoelastic strain, nor the phase of atmospheric pressure at the location of the VolcArray, are known. That said, the phase alignment with tides and the superior match of the semidiurnal spectral peaks suggests that the semidiurnal variations in *dv/v* are mainly of a tidal origin.

3.4.3. Diurnal

The main diurnal spectral peaks of *dv/v*, tidal, thermal, and tilt overlap. Upon closer inspection, however, we note that the tilt spectrum peaks at 1 cycle per day (i.e., at the thermal peak) whereas the *dv/v* peak falls in between the main tidal (and thermal) peak close to 1 cycle per day and a smaller tidal peak at slightly lower frequency. Time-domain filtering in the diurnal band reveals a substantial phase difference between *dv/v* and the tidal model (Figure 4b), although we cannot determine the phase difference between *dv/v* and thermal strain. This phase relationship indicates that the diurnal *dv/v* is not dominated by tides. With the caveat of the complex shapes of and relationships between the *dv/v*, tides, and temperature spectra, the daily variations in *dv/v* are most likely due to a superposition of tidal and thermal effects, perhaps dominated by the latter.

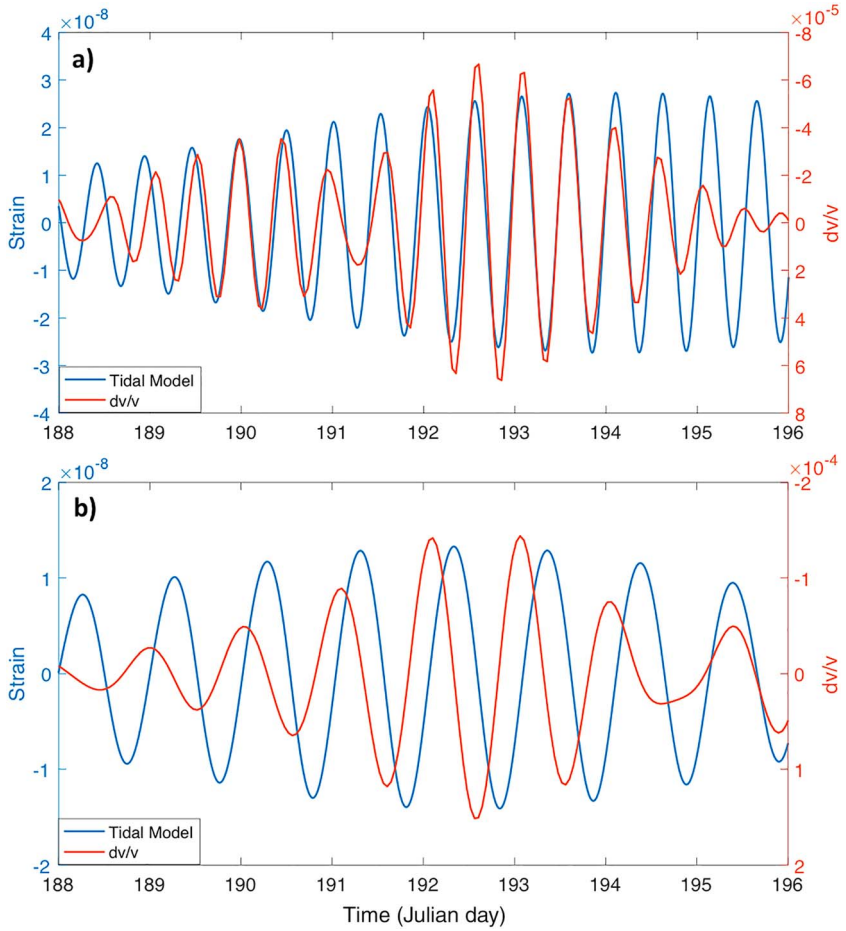


Figure 4. Comparisons of time series of tidal model and *dv/v*. Tide-induced volumetric strain and *dv/v* are (a) filtered around semidiurnal between 10 and 14 hr and (b) filtered around diurnal between 18 and 29 hr. The data are plotted for Julian days 188–196, when the nearby precipitation is low (Figure 2b), and both the diurnal and semidiurnal *dv/v* energy are relatively strong or well recovered (Figure 2c).

4. Discussions

4.1. Relative Magnitudes of Tide-Induced and Temperature-Induced Strain

The above observations suggest that both tides and solar radiation influence *dv/v* and that the relative effects depend on frequency: thermal effects dominate in the terdiurnal band, tides in the semidiurnal band, and both temperature and tides influence *dv/v* in the diurnal band. To understand the implications for crustal strain, we estimate here the tide-induced and temperature-induced strains and compare their relative magnitudes with the observed effects on *dv/v*.

SPOTL simulations suggest that at diurnal frequencies the tide-induced volumetric strain is ~10^{-8}. Temperature-induced strain is more difficult to constrain, but we can estimate the order of magnitude (see the supporting information for more details): for diurnal frequencies the thermoelastic strain is ~10^{-8}, and the strain due to temperature-caused changes of atmospheric loading is roughly 1 order smaller. This suggests that the diurnal tide-induced and temperature-induced strains are of similar magnitudes, which is consistent with our inference from the spectra that daily variations in *dv/v* have a mixed origin.

The estimation of absolute thermal strain is fraught with uncertainty, but we can use the predicted diurnal tide-induced and temperature-induced strain (which are of similar magnitude) as a starting point for relative amplitude estimation in the semidiurnal band. SPOTL simulations (Figure 3b) suggest that the semi diurnal tidal peak is larger than the diurnal peak, and the semidiurnal thermoelastic strain has been suggested to be smaller than the diurnal one (Ben-Zion & Leary, 1986). Combined, these calculations thus predict that

semidiurnal tidal strain should be larger than semidiurnal thermoelastic strain, which agrees with our empirical evidence that the semidiurnal tidal effect on *dv/v* is larger than the thermal effect.

For the terdiurnal variations we follow similar qualitative reasoning. Near 3 cycles per day, the tide-induced strain is approximately an order of magnitude smaller than around the diurnal frequency, whereas model predictions suggest that the temperature-induced strain at diurnal and ter-diurnal frequencies are of the same order. These expectations from strain modeling are consistent with the observation that the thermal effects dominate in the terdiurnal variations of *dv/v*.

4.2. Seismic Velocity Susceptibility

With the precision reached in this experiment we can evaluate the ratio between the measured magnitude of *dv/v* and stress estimated from the tidal models. During periods when the precipitation are low (that is, Julian days 188–196; Figure 2b) the seismic susceptibility is ~5×10^{-7} Pa^{-1} for the semidiurnal tide. This quantity, which can be used to characterize the mechanical state of the rocks (Brenguier et al., 2014), had previously been determined for tidal strain only by expensive active source experiments (Reasenberg & Aki, 1974; Yamamura et al., 2003). Our analysis demonstrates that with knowledge of the predictable continuous external forcings (such as tides), this can be done continuously using ambient noise records, thus enabling cost-effective long-term monitoring of the mechanical state of crustal rocks.

4.3. Depth Sensitivity of *dv/v* Measurements

For the measurements of *dv/v* we use coda waves in the 1- to 5-Hz range and a 4- to 25-s lapse time window. This part of coda contains both surface wave and body waves (conversions between the two wave types are by scattering; Hennino et al., 2001). Thus, the sensitivities of both wave types contribute to the depth sensitivity of coda-based measurements, with a partition coefficient between them depending on the lapse-time and scattering properties (Obermann et al., 2013, 2016). Under the diffusion approximation, we can evaluate the depth sensitivity of body waves following Pacheco and Snieder (2005; see the supporting information). With a mean free path l of ~0.7 km and a bulk wave velocity c of ~1.5 km/s (at lapse time around 15 s), the sensitivity of the body waves at ~2 km has reduced to 10% of the value at surface. The surface wave sensitivity decays more rapidly with depth, and vanishes after two thirds of the central wavelength, which in this case is ~500 m. The ratio of lapse time over mean free time is about 30, which corresponds to a partition coefficient of about 0.9 (Obermann et al., 2016). We conclude that our *dv/v* measurements are dominated by body wave sensitivity and therefore are most sensitive to changes within the top ~2 km.

5. Conclusions

In this study, we demonstrate the feasibility of near-real-time monitoring of small transient deformations in the shallow crust with dense arrays of autonomous seismometers. Using ambient noise, we detect daily and subdaily *dv/v* changes of the order of 0.01% (corresponding to crustal strain variations of the order of 10^{-8}, which is equivalent to stress variations of the order of 10^2 Pa with a bulk modulus of 2×10^{10} Pa) with hourly temporal resolution. The seismic susceptibility obtained here is comparable with results using active sources. Monitoring with such high precision and temporal resolution may be used to detect the precursory small deformation that is expected to occur before the onset of instabilities that are responsible for earthquakes, landslides ,and volcanic eruptions, and is therefore instrumental in the forecasting of catastrophic geological events. Furthermore, comparison and assessment of *dv/v*, theoretical modeling, and observations of Earth surface deformation suggest that the *dv/v* monitoring by dense seismic arrays provides complementary information to and can be used in concert with existing geodetic techniques, for understanding and detecting transient crustal deformation.

Acknowledgments
We thank Aurélien Mordret, Ludovic Moreau, Thomas Herring, Nori Nakata, and Qingyu Wang for helpful discussions. We thank two anonymous reviewers for their thoughtful comments and Lucy Flesch for her editorial efforts. This project has received funding from the European Research Council (ERC) under the European Union's Horizon 2020 Research and Innovation Program (grant agreement 742335, F-IMAGE). The VolcArray Experiment was funded by Foundation Simone and Cino Del Duca (Institut de France). G. Hillers acknowledges support through a Heisenberg Fellowship from the German Research Foundation (HI 1714/1-2). The authors declare that they have no competing interests. The VolcArray data were collected by the Institut des Sciences de la Terre, Observatoire Volcanologique du Piton de la Fournaise/Institut de Physique du Globe de Paris, within the framework of the VolcArray Experiment. The seismic data and metadata are available from the RESIF and EIDA data centers under the FDSN network code XP (doi: 10.15778/RESIF.XP2014). Data of broadband station RER were provided by the FDSN/Geoscope network. The tiltmeter data are provided by Observatoire Volcanologique du Piton de la Fournaise/Institut de Physique du Globe de Paris and are available at http://volobsis.ipgp.fr/. The meteorological data were provided by Météo-France.

References

Agnew, D. C. (2012). SPOTL: Some programs for ocean-tide loading. https://igppweb.ucsd.edu/~agnew/Spotl/spotlmain.html

Battaglia, J., Aki, K., & Montagner, J. P. (2000). Tilt signals derived from a GEOSCOPE VBB station on the Piton de la Fournaise volcano. *Geophysical Research Letters*, *27*(5), 605–608. https://doi.org/10.1029/1999GL010916

Ben-Zion, Y., & Leary, P. (1986). Thermoelastic strain in a half-space covered by unconsolidated material. *Bulletin of the Seismological Society of America*, *76*(5), 1447–1460.

Berger, J. (1975). A note on thermoelastic strains and tilts. *Journal of Geophysical Research*, *80*(2), 274–277. https://doi.org/10.1029/JB080i002p00274

Bouchon, M., Karabulut, H., Aktar, M., Özalaybey, S., Schmittbuhl, J., & Bouin, M. P. (2011). Extended nucleation of the 1999 Mw 7.6 Izmit earthquake. *Science*, *331*(6019), 877–880. https://doi.org/10.1126/science.1197341

Brenguier, F., Campillo, M., Hadziioannou, C., Shapiro, N. M., Nadeau, R. M., & Larose, E. (2008). Postseismic relaxation along the San Andreas fault at Parkfield from continuous seismological observations. *Science*, *321*(5895), 1478–1481. https://doi.org/10.1126/science.1160943

Brenguier, F., Campillo, M., Takeda, T., Aoki, Y., Shapiro, N. M., Briand, X., et al. (2014). Mapping pressurized volcanic fluids from induced crustal seismic velocity drops. *Science*, *345*(6192), 80–82. https://doi.org/10.1126/science.1254073

Brenguier, F., Kowalski, P., Ackerley, N., Nakata, N., Boué, P., Campillo, M., et al. (2016). Toward 4D noise-based seismic probing of volcanoes: Perspectives from a large-N experiment on Piton de la Fournaise volcano. *Seismological Research Letters*, *87*(1), 15–25. https://doi.org/10.1785/0220150173

Brenguier, F., Shapiro, N. M., Campillo, M., Ferrazzini, V., Duputel, Z., Coutant, O., & Nercessian, A. (2008). Towards forecasting volcanic eruptions using seismic noise. *Nature Geoscience*, *1*(2), 126–130. https://doi.org/10.1038/ngeo104

Campillo, M., & Paul, A. (2003). Long-range correlations in the diffuse seismic coda. *Science*, *299*(5606), 547–549. https://doi.org/10.1126/science.1078551

Chaput, J., Campillo, M., Aster, R. C., Roux, P., Kyle, P. R., Knox, H., & Czoski, P. (2015). Multiple scattering from icequakes at Erebus volcano, Antarctica: Implications for imaging at glaciated volcanoes. *Journal of Geophysical Research: Solid Earth*, *120*, 1129–1141. https://doi.org/10.1002/2014JB011278

Clarke, D., Zaccarelli, L., Shapiro, N. M., & Brenguier, F. (2011). Assessment of resolution and accuracy of the Moving Window Cross Spectral technique for monitoring crustal temporal variations using ambient seismic noise. *Geophysical Journal International*, *186*(2), 867–882.

Colombi, A., Chaput, J., Brenguier, F., Hillers, G., Roux, P., & Campillo, M. (2014). On the temporal stability of the coda of ambient noise correlations. *Comptes Rendus Geoscience*, *346*(11-12), 307–316. https://doi.org/10.1016/j.crte.2014.10.002

Donaldson, C., Caudron, C., Green, R. G., Thelen, W. A., & White, R. S. (2017). Relative seismic velocity variations correlate with deformation at Kīlauea volcano. *Science Advances*, *3*(6), e1700219. https://doi.org/10.1126/sciadv.1700219

Egbert, G. D., & Erofeeva, S. Y. (2002). Efficient inverse modeling of barotropic ocean tides. *Journal of Atmospheric and Oceanic Technology*, *19*(2), 183–204. https://doi.org/10.1175/1520-0426(2002)019<0183:EIMOBO>2.0.CO;2

Froment, B., Campillo, M., Chen, J. H., & Liu, Q. Y. (2013). Deformation at depth associated with the 12 May 2008 Mw 7.9 Wenchuan earthquake from seismic ambient noise monitoring. *Geophysical Research Letters*, *40*, 78–82. https://doi.org/10.1029/2012GL053995

Hadziioannou, C., Larose, E., Baig, A., Roux, P., & Campillo, M. (2011). Improving temporal resolution in ambient noise monitoring of seismic wave speed. *Journal of Geophysical Research*, *116*, B07304. https://doi.org/10.1029/2011JB008200

Hadziioannou, C., Larose, E., Coutant, O., Roux, P., & Campillo, M. (2009). Stability of monitoring weak changes in multiply scattering media with ambient noise correlation: Laboratory experiments. *The Journal of the Acoustical Society of America*, *125*(6), 3688–3695. https://doi.org/10.1121/1.3125345

Hennino, R., Trégourès, N., Shapiro, N. M., Margerin, L., Campillo, M., Van Tiggelen, B. A., & Weaver, R. L. (2001). Observation of equipartition of seismic waves. *Physical Review Letters*, *86*(15), 3447–3450. https://doi.org/10.1103/PhysRevLett.86.3447

Hillers, G., Ben-Zion, Y., Campillo, M., & Zigone, D. (2015). Seasonal variations of seismic velocities in the San Jacinto fault area observed with ambient seismic noise. *Geophysical Journal International*, *202*(2), 920–932. https://doi.org/10.1093/gji/ggv151

Hillers, G., Retailleau, L., Campillo, M., Inbal, A., Ampuero, J. P., & Nishimura, T. (2015). In situ observations of velocity changes in response to tidal deformation from analysis of the high-frequency ambient wavefield. *Journal of Geophysical Research: Solid Earth*, *120*, 210–225. https://doi.org/10.1002/2014JB011318

Johnson, P. A., & Jia, X. (2005). Nonlinear dynamics, granular media and dynamic earthquake triggering. *Nature*, *437*(7060), 871–874. https://doi.org/10.1038/nature04015

Melchior, P. (1974). Earth tides. *Geophysical Surveys*, *1*(3), 275–303. https://doi.org/10.1007/BF01449116

Mordret, A., Mikesell, T. D., Harig, C., Lipovsky, B. P., & Prieto, G. A. (2016). Monitoring Southwest Greenland's ice sheet melt with ambient seismic noise. *Science Advances*, *2*(5), e1501538. https://doi.org/10.1126/sciadv.1501538

Moreau, L., Stehly, L., Boué, P., Lu, Y., Larose, E., & Campillo, M. (2017). Improving ambient noise correlation functions with an SVD-based Wiener filter. *Geophysical Journal International*, *211*(1), 418–426. https://doi.org/10.1093/gji/ggx306

Nakata, N., Boué, P., Brenguier, F., Roux, P., Ferrazzini, V., & Campillo, M. (2016). Body and surface wave reconstruction from seismic noise correlations between arrays at Piton de la Fournaise volcano. *Geophysical Research Letters*, *43*, 1047–1054. https://doi.org/10.1002/2015GL066997

Obermann, A., Planès, T., Hadziioannou, C., & Campillo, M. (2016). Lapse-time-dependent coda-wave depth sensitivity to local velocity perturbations in 3-D heterogeneous elastic media. *Geophysical Journal International*, *207*(1), 59–66. https://doi.org/10.1093/gji/ggw264

Obermann, A., Planès, T., Larose, E., Sens-Schönfelder, C., & Campillo, M. (2013). Depth sensitivity of seismic coda waves to velocity perturbations in an elastic heterogeneous medium. *Geophysical Journal International*, *194*(1), 372–382. https://doi.org/10.1093/gji/ggt043

Olivier, G., Brenguier, F., Campillo, M., Roux, P., Shapiro, N. M., & Lynch, R. (2015). Investigation of coseismic and postseismic processes using in situ measurements of seismic velocity variations in an underground mine. *Geophysical Research Letters*, *42*, 9261–9269. https://doi.org/10.1002/2015GL065975

Pacheco, C., & Snieder, R. (2005). Time-lapse travel time change of multiply scattered acoustic waves. *The Journal of the Acoustical Society of America*, *118*(3), 1300–1310. https://doi.org/10.1121/1.2000827

Pillet, R., & Virieux, J. (2007). The effects of seismic rotations on inertial sensors. *Geophysical Journal International*, *171*(3), 1314–1323. https://doi.org/10.1111/j.1365-246X.2007.03617.x

Poupinet, G., Ellsworth, W. L., & Frechet, J. (1984). Monitoring velocity variations in the crust using earthquake doublets: An application to the Calaveras fault, California. *Journal of Geophysical Research*, *89*(B7), 5719–5731. https://doi.org/10.1029/JB089iB07p05719

Rabbel, W., & Zschau, J. (1985). Static deformations and gravity changes at the Earth's surface due to atmospheric loading. *Journal of Geophysics- Zeitschrift fuer Geophysik*, *56*, 81–89.

Reasenberg, P., & Aki, K. (1974). A precise, continuous measurement of seismic velocity for monitoring in situ stress. *Journal of Geophysical Research*, *79*(2), 399–406. https://doi.org/10.1029/JB079i002p00399

Richter, T., Sens-Schönfelder, C., Kind, R., & Asch, G. (2014). Comprehensive observation and modeling of earthquake and temperature-related seismic velocity changes in northern Chile with passive image interferometry. *Journal of Geophysical Research: Solid Earth*, *119*, 4747–4765. https://doi.org/10.1002/2013JB010695

Rivet, D., Brenguier, F., & Cappa, F. (2015). Improved detection of preeruptive seismic velocity drops at the Piton de La Fournaise volcano. *Geophysical Research Letters*, *42*, 6332–6339. https://doi.org/10.1002/2015GL064835

Rivet, D., Campillo, M., Shapiro, N. M., Cruz-Atienza, V., Radiguet, M., Cotte, N., & Kostoglodov, V. (2011). Seismic evidence of nonlinear crustal deformation during a large slow slip event in Mexico. *Geophysical Research Letters*, *38*, L08308. https://doi.org/10.1029/2011GL047151

Sabra, K. G., Gerstoft, P., Roux, P., Kuperman, W. A., & Fehler, M. C. (2005). Extracting time-domain Green's function estimates from ambient seismic noise. *Geophysical Research Letters*, *32*, L03310. https://doi.org/10.1029/2004GL021862

Scuderi, M. M., Marone, C., Tinti, E., Di Stefano, G., & Collettini, C. (2016). Precursory changes in seismic velocity for the spectrum of earthquake failure modes. *Nature Geoscience*, *9*(9), 695–700. https://doi.org/10.1038/ngeo2775

Sens-Schönfelder, C., & Wegler, U. (2006). Passive image interferometry and seasonal variations of seismic velocities at Merapi Volcano, Indonesia. *Geophysical Research Letters*, *33*, L21302. https://doi.org/10.1029/2006GL027797

Shapiro, N. M., & Campillo, M. (2004). Emergence of broadband Rayleigh waves from correlations of the ambient seismic noise. *Geophysical Research Letters*, *31*, L07614. https://doi.org/10.1029/2004GL019491

Snieder, R., Grêt, A., Douma, H., & Scales, J. (2002). Coda wave interferometry for estimating nonlinear behavior in seismic velocity. *Science*, *295*(5563), 2253–2255. https://doi.org/10.1126/science.1070015

Stehly, L., Froment, B., Campillo, M., Liu, Q. Y., & Chen, J. H. (2015). Monitoring seismic wave velocity changes associated with the Mw 7.9 Wenchuan earthquake: Increasing the temporal resolution using curvelet filters. *Geophysical Journal International*, *201*(3), 1939–1949. https://doi.org/10.1093/gji/ggv110

Takano, T., Nishimura, T., Nakahara, H., Ohta, Y., & Tanaka, S. (2014). Seismic velocity changes caused by the Earth tide: Ambient noise correlation analyses of small-array data. *Geophysical Research Letters*, *41*, 6131–6136. https://doi.org/10.1002/2014GL060690

Talwani, P., Chen, L., & Gahalaut, K. (2007). Seismogenic permeability, ks. *Journal of Geophysical Research*, *112*, B07309. https://doi.org/10.1029/2006JB004665

Tape, C., Holtkamp, S., Silwal, V., Hawthorne, J., Kaneko, Y., Ampuero, J. P., et al. (2018). Earthquake nucleation and fault slip complexity in the lower crust of central Alaska. *Nature Geoscience*, *1*. https://doi.org/10.1038/s41561-018-0144-2

Tsai, V. C. (2011). A model for seasonal changes in GPS positions and seismic wave speeds due to thermoelastic and hydrologic variations. *Journal of Geophysical Research*, *116*, B04404. https://doi.org/10.1029/2010JB008156

Walsh, J. B. (1965). The effect of cracks on the compressibility of rock. *Journal of Geophysical Research*, *70*(2), 381–389. https://doi.org/10.1029/JZ070i002p00381

Wang, B., Zhu, P., Chen, Y., Niu, F., & Wang, B. (2008). Continuous subsurface velocity measurement with coda wave interferometry. *Journal of Geophysical Research*, *113*, B12313. https://doi.org/10.1029/2007JB005023

Wang, J., Tilmann, F., White, R. S., Soosalu, H., & Bordoni, P. (2008). Application of multichannel wiener filters to the suppression of ambient seismic noise in passive seismic arrays. *The Leading Edge*, *27*(2), 232–238. https://doi.org/10.1190/1.2840372

Wang, Q. Y., Brenguier, F., Campillo, M., Lecointre, A., Takeda, T., & Aoki, Y. (2017). Seasonal crustal seismic velocity changes throughout Japan. *Journal of Geophysical Research: Solid Earth*, *122*, 7987–8002. https://doi.org/10.1002/2017JB014307

Weaver, R. L., Hadziioannou, C., Larose, E., & Campillo, M. (2011). On the precision of noise correlation interferometry. *Geophysical Journal International*, *185*(3), 1384–1392. https://doi.org/10.1111/j.1365-246X.2011.05015.x

Yamamura, K., Sano, O., Utada, H., Takei, Y., Nakao, S., & Fukao, Y. (2003). Long-term observation of in situ seismic velocity and attenuation. *Journal of Geophysical Research*, *108*(B6), 2317. https://doi.org/10.1029/2002JB002005

Zhan, Z., Tsai, V. C., & Clayton, R. W. (2013). Spurious velocity changes caused by temporal variations in ambient noise frequency content. *Geophysical Journal International*, *194*(3), 1574–1581. https://doi.org/10.1093/gji/ggt170